An Accelerated Unstructured Multigrid Method for Shells

J. Fish, L. Pan, V. Belsky and S. Gomaa
Department of Civil Engineering and Scientific Computation Research Center
Rensselaer Polytechnic Institute, Troy, NY 12180

ABSTRACT

An accelerated multigrid method, which exploits shell element formulation to speed up the iterative process, is developed for inherently poor conditioned thin domain problems on unstructured grids. Its building blocks are: (i) intergrid transfer operators based on the shell element shape functions, (ii) heavy smoothing procedures in the form of Modified Incomplete Cholesky factor, and (iii) various two- and three-parameter acceleration schemes. Both the flat shell triangular element and the assumed strain degenerated solid shell element are considered. Numerical results show a remarkable robustness for a wide spectrum of span/thickness ratios encountered in practical applications.

1.0 Introduction

This paper focuses on development of efficient iterative solvers for a linear system of equations arising from the finite element discretization of large scale shell structures. On one hand, iterative methods, such as preconditioned conjugate gradient (PCG) and multigrid (MG), offer the promise of substantially reducing operations and storage requirements for large scale systems, but on the other hand, they are not well suited for inherently poor conditioned thin domain problems, such as thin shells.

It is often assumed that for well conditioned three-dimensional problems the number of degrees-of-freedom for which the conjugate gradient method requires the same amount of CPU time as the direct method is in the neighborhood of 500, while a breakeven problem size for the multigrid method is approximately double [1], [2]. There is no doubt that the breakeven problem size for shells will move upwards as the span/thickness ratio increases. This paper attempts to assess the balance between a problem size and a thickness/span ratio that will justify the use of either iterative or direct solvers.

We focus on the accelerated multigrid method for shells, which offers the advantage of possessing an asymptotically optimal rate of convergence with linear complexity, i.e., computational work for achieving a prescribed accuracy is proportional to the number of discrete unknowns. It is important to note that the overhead involved in automatic mesh generation of the hierarchy of auxiliary surface meshes needed for multigrid applications is relatively small in comparison to the total solution time for large thin domain problems,

where a breakeven problem size might be very high.

Since the pioneering work of Fedorenko [3] in 1962, multigrid literature has grown at an astonishing rate. A cumulative review of the technical literature may be found in the Multigrid Bibliography [4], which is periodically updated. Applications of unstructured multigrid method have been typically concentrated in fluid mechanics, with very few attempts in solid mechanics [1], [5], [6], [7], [8], [9]. To our knowledge this is one of the first attempts aimed at investigating the usefulness of the multigrid method for solving a system of discrete equations arising from the finite element discretization of shells. The noteworthy exceptions are the PCG method with incomplete blockwise factorization preconditioner, which can be interpreted as a nested two-grid method[10], and the application of the multigrid method to hierarchical shell systems (p-method) [11], where the multigrid-like solvers are most natural due to the simplicity of intergrid transfer operators, which are simply identity operators.

One of our key goals is to examine the influence of various formulations of the primary multigrid elements, such as coarse grid correction, smoothing or relaxation procedures, intergrid transfer operators, and acceleration schemes, on the overall performance of the iterative process. In section 2, we examine several formulations of intergrid transfer (prolongation and restriction) operators for each of the two shell theories: (i) flat elements, formed by combining a plane membrane element with a plate bending element, and (ii) degenerated solid elements with certain kinematic and mechanical assumptions built in. In the first category we consider the 18 degrees-of-freedom flat shell triangular element [12], [13], which is based on the superposition of the DKT plate element [14] and the membrane element with drilling degrees-of-freedom [15], while the curved 9-node ANS element [16]is used as a representative of the second category.

2.0 The Multigrid Algorithm

As a prelude to subsequent derivations we briefly outline the basic two-grid algorithm for solving a linear systems of equations resulting from the finite element discretization

$$K_{AB}d_B = f_B \tag{1}$$

where capital subscripts are reserved for degrees-of-freedom in the source grid. Tensorial convention is employed with summation over the repeated indices.

The two-grid method summarized below is an iterative process that resolves higher frequency response of the system by means of relaxation methods, while the remaining smooth components of the solution are captured on the auxiliary coarse grid.

- Starting from the source (fine) grid approximation d_B^i, which is obtained at the end of cycle i, perform typically one or two pre-smoothing iterations to smooth out high frequency components of the error and evaluate the fine grid residual r_A
- Restrict the residual from the fine grid to the auxiliary coarse grid

$$r_a = Q_{aA}r_A \tag{2}$$

where lower case subscripts denote the degrees-of-freedom in the auxiliary coarse grid and Q_{aA} is the restriction operator

- Compute the coarse grid correction Δd_b

$$K_{ab}\Delta d_b = r_a \tag{3}$$

where K_{ab} is the coarse grid stiffness matrix obtained either directly on the auxiliary coarse grid or by restricting the fine grid stiffness matrix

$$K_{ab} = Q_{aA}K_{AB}Q_{Bb} \tag{4}$$

The solution of Equation (3) can be carried out by a direct solver, or, if this is still too expensive, by introducing another coarser auxiliary grid and using one or more cycles of the two-grid algorithm.

- Prolongate the displacement correction from the coarse grid to the fine grid and update

$$d_B \Leftarrow d_B + \omega Q_{Bb}\Delta d_b \tag{5}$$

where Q_{Bb} is termed as prolongation operator related to the restriction operator by $\left[Q_{Bb}\right] = \left[Q_{bB}\right]^T$, and ω is a coarse grid relaxation parameter, which minimizes energy functional along the prescribed direction $\Delta d_B = Q_{Bb}\Delta d_b$. Note that $\omega = 1$ for two grid problems, where the coarse grid stiffness matrix is obtained by restriction (4); otherwise,

$$\omega = \frac{\Delta d_B r_B}{\Delta d_C K_{CA}\Delta d_A} \tag{6}$$

- Perform post-smoothing operations starting with the updated solution on the fine grid to obtain a new approximation d_B^{i+1}
- Accelerate the multigrid cycle using two-parameter scheme:

$$d_B^{i+1} \Leftarrow d_B^i + \alpha\left(d_B^{i+1} - d_B^i\right) + \beta\left(d_B^i - d_B^{i-1}\right) \tag{7}$$

where α and β are step sizes (in the corresponding search directions) selected on the basis of minimizing the energy functional. The alternative acceleration scheme in the form of conjugate gradients is briefly described in section 4.

- Check convergence. If necessary, start a new cycle.

The building blocks of the accelarated multigrid algorithm, including (i) the intergrid transfer operators, (ii) smoothing schemes, (iii) coarse grid correction and (iv) acceleration, will be investigated in the subsequent sections.

3.0 The Intergrid Transfer Operators for Shells

3.1 Flat shell triangular element

We consider an 18 degrees-of-freedom flat shell triangular element [12], [13], which is based on the superimposition of the DKT plate element [14] and the membrane plane stress element with drilling degrees-of-freedom [15], subsequently to be referred to as the Discrete Membrane Triangle (DMT).

3.1.1 The DKT Plate Bending Element

The DKT plate bending element is a Discrete Kirchhoff Triangle which satisfies the Kirchhoff hypothesis at some discrete points within the element. For element formulation we refer to [14]. In this section we briefly outline only those element formulation details which are relevant to the construction of intergrid transfer operators.

Let β_1 and β_2 be the rotations of the normal to the midsurface in the local element coordinate system and $\{d_{a'}\}^T = \left[w_1\ \theta_{x_1}\ \theta_{y_1}\ w_2\ \theta_{x_2}\ \theta_{y_2}\ w_3\ \theta_{x_3}\ \theta_{y_3}\right]$ be the nodal degrees-of-freedom of the element corresponding to out-of-plane displacements and midplane rotations, which are related by the set of shape functions $H_{a'}^{\beta_1}$ and $H_{a'}^{\beta_2}$ described in Appendix A.

$$\beta_1 = H_{a'}^{\beta_1} d_{a'} \qquad \beta_2 = H_{a'}^{\beta_2} d_{a'} \qquad \text{.....sum on } a' = [1,9] \tag{8}$$

where the prime on the subscript denotes the quantities with respect to the element local coordinate system.

Let x_A be the coordinates of the node in the source mesh, which lies within one of the auxiliary coarse mesh elements. Then the nodal rotations in the source mesh can be found directly from (8)

$$\theta_1(x_A) = -H_{a'}^{\beta_2}(x_A)\, d_{a'} \qquad \theta_2(x_A) = H_{a'}^{\beta_1}(x_A)\, d_{a'} \quad \text{.....sum on } a' = [1,9] \tag{9}$$

Unfortunately, for the DKT element the transverse displacement w in the interior of the element is not defined [14], since the transverse shear energy is neglected in the element formulation and therefore auxiliary interpolation function for w needs to be constructed. We assume that w is a quadratic field, with shape functions corresponding to three vertex and three midside modes. The midside translations w_4 w_5 and w_6 are found using the cubic variation of w along each side (see Appendix A), which yields

$$w(x_A) = H_{a'}^{w}(x_A)\, d_{a'} \quad \text{.....sum on } a' = [1,9] \tag{10}$$

3.1.2 The DMT Membrane Element

The Discrete Membrane Triangular (DMT) shell element is a 9 degrees-of-freedom plane stress element, which interpolates the in-plane translation field u and v in terms of in-plane translations and drilling rotations at the element vertices

$$u = H^{u}_{a'} d_{a'} \qquad v = H^{v}_{a'} d_{a'} \quad \text{.....sum on } a' = [1,9] \tag{11}$$

where $\{d_{a'}\}^T = \left[u_1\ v_1\ \theta_{Z_1}\ u_2\ v_2\ \theta_{Z_2}\ u_3\ v_3\ \theta_{Z_3}\right]$ is the nodal displacement vector, $H^{u}_{a'}$ and $H^{v}_{a'}$ are the corresponding shape functions described in Appendix A.

As in the DKT element where the transverse displacement field is not defined, in the DMT a similar situation exists for the rotational(drilling) field with respect to the normal to the element plane. We will construct a linear interpolation for drilling degrees-of-freedom.

3.1.3 The Intergrid Transfer Operators For DKT+DMT Shell Element

Based on (9), (10), (11) and (12), and after proper assembly we obtain

$$\boldsymbol{d}_{A'} = \boldsymbol{Q}_{A'a'} \boldsymbol{d}_{a'} \tag{12}$$

in which $\boldsymbol{d}_{A'}$ and $\boldsymbol{d}_{a'}$ are local nodal vectors in the source and auxiliary meshes, respetively

$$\boldsymbol{d}_{A'} = \left[u_{A'}\ v_{A'}\ w_{A'}\ \theta_{1A'}\ \theta_{2A'}\ \theta_{3A'}\right] \qquad \boldsymbol{d}_{a'} = \left[u_{a'}\ v_{a'}\ w_{a'}\ \theta_{1a'}\ \theta_{2a'}\ \theta_{3a'}\right] \tag{13}$$

A Similar relation can be constructed for nodal vectors given in the global coordinate system

$$\boldsymbol{d}_{A} = \boldsymbol{Q}_{Aa} \boldsymbol{d}_{a} \tag{14}$$

where

$$\boldsymbol{Q}_{\underline{Aa}} = \boldsymbol{T}_{\underline{AA'}} \boldsymbol{Q}_{\underline{A'a'}} \boldsymbol{T}^{T}_{\underline{aa'}} \quad \text{.....no summation over the underlined indices} \tag{15}$$

$\boldsymbol{T}_{AA'}$ and $\boldsymbol{T}_{aa'}$ are local-to-global orthogonal transformation matrices in the source and auxiliary meshes, respectively.

Remark 1: An alternative to the prolongation operator defined on the basis of the element shape functions (8)-(16) one can simply employ a linear interpolation for translational and rotational degrees-of-freedom using classical constant strain triangle shape functions, but as will be shown in section 5, the efficiency will suffer.

Remark 2: In order to construct the intergrid transfer operator given in (15) for general unstructured (unnested) grids it is important to employ an efficient method for collecting and interpolating information from one grid to another. The goal is to find in which coarse grid element each fine grid node lies as well as fine grid local coordinates in the coarse element. This operation can be easily accomplished by looping over all fine grid nodes and coarse grid elements, in which case the search procedure may overshadow the entire

computational cost. A more economical procedure can be obtained by introducing the background grid [17]. For uniformly shaped source grids, the background grid consists of equally-sided brick elements filling the rectangular frame encompassing the entire problem domain. The total number of bricks in the background grid is taken to be equal to the number of elements in the auxiliary coarse grid. The search algorithm consists of two steps: (i) For each point in the source grid, determine in which brick element in the background grid it lies. Store the brick number and count the number of source grid points in each brick. (ii) For each element in the auxiliary coarse grid, determine which bricks in the background grid it covers and check if the corresponding source grid points lie within this element; if they do, calculate the local coordinates; if not, proceed to the next element.

3.2 The ANS Shell Element

The ANS shell is based on a Mindlin/Reissner-like (C^0 continuous) degenerated-solid shell formulation with assumed natural strain formulation aimed at circumvent locking and reduce distortion sensitivity [16].

The displacement field of the ANS element is of the classical degenerated solid type

$$\boldsymbol{u}(\xi,\eta,\zeta) = \sum_{a=1}^{n_{en}} N_a(\xi,\eta)\left[\ \bar{\boldsymbol{u}}_a + \frac{1}{2}\zeta h_a\left(\theta_{a2}\boldsymbol{e}^f_{a1} - \theta_{a1}\boldsymbol{e}^f_{a2}\right)\ \right] \tag{16}$$

where $\bar{\boldsymbol{u}}_a$ are nodal translations at the reference surface; $\boldsymbol{e}^f_{a1}, \boldsymbol{e}^f_{a2}, \boldsymbol{e}^f_{a3}$ are orthonormal fiber basis vector at node a, defined so that $\boldsymbol{e}^f_{a3}$ is normal to the plane and $\boldsymbol{e}^f_{a1}, \boldsymbol{e}^f_{a2}$ are as close as possible to the ξ, η coordinate directions; θ_{a1}, θ_{a2} are rotations of the fiber about the basis vectors $\boldsymbol{e}^f_{a1}, \boldsymbol{e}^f_{a2}$, respectively; h_a is the thickness of the shell at node a; $N_a(\xi,\eta)$ are the in-plane n_{en} Lagrangian shape functions.

The prolongation operator for the translational degrees-of-freedom can be directly obtained from the above Lagrangian shape functions

$$\bar{\boldsymbol{u}}_A = N_a(x_A)\,\bar{\boldsymbol{u}}_a \text{.....sum on } a = [1,9] \tag{17}$$

To construct the prolongation operator for the rotational degrees-of-freedom, we first evaluate the relative displacement in the source mesh

$$\Delta\boldsymbol{u}(x_A) = \boldsymbol{u}^{top}(x_A) - \boldsymbol{u}^{bot}(x_A) = \begin{bmatrix}\Delta u_x\\ \Delta u_y\\ \Delta u_z\end{bmatrix}_{x_A} = \sum_{a=1}^{n_{en}} N_a(x_A)\ h_a\left(\theta_{a2}\boldsymbol{e}^f_{a1} - \theta_{a1}\boldsymbol{e}^f_{a2}\right) \tag{18}$$

which is then transformed into a local element coordinate system

$$\begin{bmatrix}\Delta u_1(x_A)\\ \Delta u_2(x_A)\end{bmatrix} = \begin{bmatrix}e_{A1,x} & e_{A1,y} & e_{A1,z}\\ e_{A2,x} & e_{A2,y} & e_{A2,z}\end{bmatrix}\begin{bmatrix}\Delta u_x\\ \Delta u_y\\ \Delta u_z\end{bmatrix}_{x_A} = e_{A\beta,k}\Delta u_k(x_A) \tag{19}$$

where $\beta = 1, 2$ is a free index, and summation over repeated indices over $k = 1, 2, 3$ is exercised. Consequently the rotational field is prolongated as follows:

$$\theta_1(x_A) = -\frac{\Delta u_2(x_A)}{h_A} = N_a^{\theta_{11}}(x_A)\,\theta_{a1} + N_a^{\theta_{12}}(x_A)\,\theta_{a2}$$

$$\theta_2(x_A) = \frac{\Delta u_1(x_A)}{h_A} = N_a^{\theta_{21}}(x_A)\,\theta_{a1} + N_a^{\theta_{22}}(x_A)\,\theta_{a2} \qquad \text{.....sum on } a = [1,9] \qquad (20)$$

where shape functions are summarized in Appendix B. The resulting node-to-node prolongation operator is given by:

$$\left[Q_{Aa}\right] = \begin{bmatrix} N_a(x_A) & 0 & 0 & 0 & 0 \\ 0 & N_a(x_A) & 0 & 0 & 0 \\ 0 & 0 & N_a(x_A) & 0 & 0 \\ 0 & 0 & 0 & N_a^{\theta_{11}}(x_A) & N_a^{\theta_{12}}(x_A) \\ 0 & 0 & 0 & N_a^{\theta_{21}}(x_A) & N_a^{\theta_{22}}(x_A) \end{bmatrix} \qquad (21)$$

Remark 3: An alternative to the prolongation operator for rotational degrees-of-freedom defined on the basis of the element shape functions (18)-(20) is to employ a Lagrangian interpolation identical to the one employed for translation degrees-of-freedom (18).

Remark 4: For higher order ANS meshes, it is convenient to construct an auxiliary mesh from lower order ANS elements. For example, the shape functions of 4-node ANS element $N_a^{4-Node}(X_A)$ can be utilized for prolongating the solution from 9-node ANS elements. Similarly, 9-node elements can serve as an auxiliary mechanism for 16-node elements, and etc.

For higher order elements an alternative, which exploits the fact that membrane dominated modes are of higher frequency than those of bending, will be tested. By this approach only membrane dominated modes of higher order elements are prolongated using lower order element shape functions, whereas bending dominated modes, for which the smoothing process is usually inefficient, are prolongated using an identity operator, and then resolved with a direct solver. Mode separation is carried out in the local fiber coordinate system, which requires transformation of all global quantities, including stiffness, displacement and force vectors from the global to the local fiber coordinate system.

Remark 5: It is important to note that in the case of assumed strain formulation, restriction of the source grid stiffness matrix, $Q_{aA}K_{AB}Q_{Bb}$, does not yield the stiffness matrix of the coarse grid independently recomputed even though the meshes are nested. This is because the assumed strain field is enhanced by projecting certain undesirable modes from the symmetric gradient of the displacement field. Whether it is more computationally efficient to construct the auxiliary coarse mesh stiffness matrix by restriction (eq. (4)) or by recomputation and coarse grid acceleration (6) will be investigated in section 5.

4.0 Acceleration schemes

For ill-conditioned problems various acceleration schemes are essential to speed up the rate of convergence. This is especially true for thin shell problems, where the auxiliary

coarse meshes might be too stiff to accurately capture the lower frequency response of the source problem. However, when both the coarse grid correction and relaxation solutions are appropriately scaled the speedup is often astonishing, by a factor of ten and more, as evident from our numerical examples.

We start by describing the so-called two-parameter acceleration scheme, which uses the incremental multigrid cycle as a search direction, and subsequently scales it to minimize the potential energy functional.

Let r_B^i be the residual at the end of cycle i. The incremental multigrid solution for the next cycle, denoted as $z_B^i = MG\left(r_B^i, K_{AB}\right)$, is used as the predictor in the two parameter acceleration scheme. The solution in the correction phase is then updated as follows:

$$v_B^{i+1} = \alpha^i z_B^i + \beta^i v_B^i \tag{22}$$

$$d_B^{i+1} = d_B^i + v_B^{i+1} \tag{23}$$

where parameters $\left(\alpha^i, \beta^i\right)$ are obtained by minimization of the potential energy functional

$$\frac{1}{2}\left(d_A^i + \alpha^i z_A^i + \beta^i v_A^i\right) K_{AB} \left(d_B^i + \alpha^i z_B^i + \beta^i v_B^i\right) - \left(d_A^i + \alpha^i z_A^i + \beta^i v_A^i\right) f_A \rightarrow \min_{\alpha^i, \beta^i} \tag{24}$$

The resulting algorithm of the two parameter acceleration scheme is summarized below:

Step 1: Initiation

$$d_B^0 = 0 \qquad r_B^0 = f_B \tag{25}$$

$$z_B^0 = MG\left(r_B^0, K_{AB}\right) \tag{26}$$

$$v_B^0 = 0 \qquad y_B^0 = 0 \tag{27}$$

$$x_B^0 = K_{BC} z_C^0 \tag{28}$$

$$\alpha^0 = \frac{z_C^0 f_C}{z_D^0 x_D^0} \qquad \beta^0 = 0 \tag{29}$$

Step 2: Do i = 0, 1, 2, ... until convergence

$$\begin{Bmatrix} \alpha^i \\ \beta^i \end{Bmatrix} = \begin{bmatrix} z_C^i x_C^i & v_A^i x_A^i \\ v_B^i x_B^i & y_D^i x_D^i \end{bmatrix}^{-1} \begin{Bmatrix} z_E^i r_E^i \\ v_F^i r_F^i \end{Bmatrix} \qquad i > 0 \tag{30}$$

$$v_B^{i+1} = \alpha^i z_B^i + \beta^i v_B^i \tag{31}$$

$$d_B^{i+1} = d_B^i + v_B^{i+1} \tag{32}$$

$$y_B^{i+1} = \alpha^i x_B^i + \beta^i y_B^i \tag{33}$$

$$r_B^{i+1} = r_B^i - y_B^{i+1} \tag{34}$$

$$z_B^{i+1} = MG\left(r_B^{i+1}, K_{AB}\right) \tag{35}$$

$$x_B^{i+1} = K_{BC} z_C^{i+1} \tag{36}$$

Note that the two parameter acceleration scheme requires no additional matrix-vector multiplication and for thin shells its benefit clearly overshadows the cost involved in additional vector product evaluations.

An alternative to the acceleration scheme described in equations (26)-(37) is the use of a multigrid cycle as a preconditioner within the conjugate gradient method

$$v_B^{i+1} = MG\left(r_B^i, K_{AB}\right) + \beta^i v_B^i \tag{37}$$

$$d_B^{i+1} = d_B^i + \alpha^i v_B^{i+1} \tag{38}$$

where the parameters α^i, β^i are determined from the line search and K-orthogonality$\left(K_{AB} v_B^i, v_A^{i+1}\right) = 0$, respectively.

5.0 Numerical examples and discussion

Our numerical experimentation agenda includes investigation of various intergrid transfer operators described in section 3 as well as other multigrid elements, such as smoothing, coarse grid correction and acceleration.

Two problems are considered, the line pinched cylinder with end diaphragms, and the assembly of three cylinders with end diaphragms subjected to point load. Geometry, loading, boundary conditions and material properties for the two problems are given in Figures 1(a) and 1(b). Uniform and graded meshes of either ANS or Flat Shell Triangular (FST) elements as shown in Tables 1 and 2, and Figures 2 and 3 have been considered. For uniform meshes, mesh 1 is used as an auxiliary grid for mesh 3, while mesh 2 is auxiliary to mesh 4. The nodes of all auxiliary and source meshes are placed on the exact geometry, which ensures an unnested situation for curved shell structures. All numerical examples were conducted for five different radius/thickness ratios: 50, 100, 200, 500 and 1000. Convergence was measured in terms of the normalized L_2-norm of the residual with tolerance of 10e-6. Computations were carried out on the SPARC 10 workstation.

For flat shell triangular element meshes four different formulations of intergrid transfer operators have been compared.

Bsh-Msh — Bending prolongated using DKT element shape functions (eqs. (8)(10)); Membrane displacements prolongated using DMT element shape functions (eqs. (11)).

Bln-Mln — Bending prolongated using linear field; Membrane prolongated using linear field.

Bsh-Mln — Bending prolongated using DKT element shape functions (eqs. (8)(10)); Membrane prolongated using linear field.

Bln-Msh — Bending prolongated using linear field; Membrane displacements prolongated using DMT element shape functions (eqs. (11)).

Tables 3 and 4 compare computational efficiency (measured in terms of CPU time and number of iterations) of various intergrid transfer operators for the two test problems. From the program architecture standpoint the use of linear basis for prolongating all the fields (Bln-Mln) is very attractive, since no information on element formulation is needed in the solution process. Nevertheless, it is evident from tables 3 and 4, that the computational efficiency of the two-grid method, which exploits the element information and in particular that of the DKT element in the iterative solution process, is by far superior. It can be seen that the optimal computational performance has been obtained with the Bsh-Mln version of the prolongation operator.

In the case of 9-node ANS elements we study the following five different formulations of the intergrid transfer operators defined as:

BiQ9 — 9-node Bi-Quadratic prolongation for midplane displacements and rotations.

BiQ9Mr — 9-node Bi-Quadratic prolongation for midplane displacements (eq. (18)). Midplane rotations are extracted from displacements (eqs.(19)(20)(21)).

BiL4 — 4-node Bi-Linear prolongation for midplane displacements and rotations, i.e. 4-node elements are used as an auxiliary mesh for 9-node elements.

MeBiL4 — Bending prolongated using an identity operator. 4-node Bi-Linear prolongation is used for Membrane only. See Remark 4.

BiQ9Re — 9-node Bi-Quadratic prolongation and restriction operators for all degrees-of-freedom. Coarse mesh stiffness matrix Recomputed and coarse grid solution accelerated using equation (6). See remark 5.

Tables 5 and 6 compare the five intergrid transfer operators for the two test problems. It is evident that the most efficient formulation is the one that recomputes the coarse grid stiffness matrix (BiQ9Re), i.e., the stiffness matrix obtained by any form of restriction fails to effectively capture the lower frequency response of the source mesh. This is not surpris-

ing, because the intergrid transfer operators are formulated on the basis of shape functions only, and do not reflect the enhanced strain field of the assumed strain element. The intergrid transfer operator, which is based on bi-linear prolongation for membrane and identity for bending, MeBiL4, yields fewer cycles, but does not offer savings in terms of the overall performance because the auxiliary mesh is larger and thus CPU time per cycle is longer.

Comparing results in Tables 3 and 4 with those in Tables 4 and 5, it can be seen that a general trend indicates a significantly faster rate of convergence of the flat shell triangular element. Similar observations have been found from the experiments conducted on the two and three level graded meshes as shown in Table 13.

Tables 7 and 8 investigate the influence of acceleration on the rate of convergence in the case of FST and ANS meshes, respectively. It can be seen that acceleration significantly affects the rate of convergence especially as the span thickness ratio increases. The two acceleration schemes, based on the conjugate gradient method and minimization of potential energy functional, described in section 4 have similar performance in terms of number of iterations and CPU time.

In Tables 9 and 10 we investigate two popular smoothing procedures based on Gauss-Seidel and Modified Incomplete Cholesky (MIC) Factorization [18] with 0.05 diagonal scaling for stabilization for both FST and ANS meshes. It is evident that for thick shells, the two smoothers have similar computational performance. For poor conditioned problems (span/thickness ratio over 500) a heavier smoothing procedure, such as MIC, is the most efficient, by far outperforming one or two Gauss-Seidel smoothing iterations.

6.0 Summary and conclusions

Recent years saw a re-emergence of iterative solvers in finite element structural analysis due to increasing demand to analyze very large finite element systems. However, the major obstacle that needs to be overcome before iterative solvers can be routinely used in commercial packages is circumventing their pathological sensitivity to problem conditioning. This paper presents an attempt in this direction in the form of an accelerated multigrid method dedicated for inherently poor conditioned thin domain problems, which exploits the knowledge of the finite element formulation in speeding up the iterative process.

Tables 11-12 compare the performance of the most efficient version of the accelerated multigrid method developed against the conjugate gradient method with Incomplete Cholesky preconditioner and the direct solver with skyline storage for the two problems and the two types of elements considered. In the case of the multigrid solver, the CPU time includes the overhead involved in the auxiliary mesh generation and the data transfer between the grids. Results show remarkable robustness of the accelerated multigrid method for a wide spectrum of span/thickness ratios encountered in practical applications as opposed to the MIC preconditioned conjugate gradient method. Nevertheless, superiority claims with respect to direct methods are premature at this point since (i) no comparisons with some of the state-of-the-art sparse direct solvers [19] have been carried out, and

(ii) no tests were conducted on large scale industry problems. Moreover, we would like to caution that for linear static analysis, any form of the multigrid method requires for each load case a new iterative process (except for the stiffness formation, restriction and factorization on the coarse grid), whereas in a direct solution, factorization is performed only once, and each load case requires only forward reduction and back substitution.

REFERENCES

1 I. D. Parsons and J. F. Hall, 'The Multigrid Method in Solid Mechanics: Part I-Algorithm Description and Behavior,' *Int. J. For Numerical Methods In Engineering,* Vol. 29, 719-737, 1990.

2 T. J. R. Hughes, R. M. Ferencz and J. O. Hallquist, 'Large scale vectorized implicit calculations in solid mechanics on a Cray X-MP/48 utilizing EBE preconditioned conjugate gradients,' *Computer Methods in Applied Mechanics and Engineering*, Vol. 61, pp. 215-248, 1987.

3 R. P. Fedorenko, 'A relaxation method for solving elliptic difference equations,' *USSR Computational Math. and Math. Phys.*, Vol. 1, No. 5, pp.1092-1096, 1962.

4 W. Hackbusch and U. Trottenberg, *Multigrid Methods*, Springer-Verlag, Berlin, 1992.

5 D. Parsons, 'Iterative methods and finite elements: when will convergence occur?,' *USACM Bulletin*, Vol. 7, No. 3, September 1994.

6 J. Fish and V.Belsky, 'Multigrid method for periodic heterogeneous media. Part I: Convergence studies for one-dimensional case,' accepted in *Computer Methods in Applied Mechanics and Engineering.*

7 J.Fish and V.Belsky, 'Multigrid method for periodic heterogeneous media. Part II: Multiscale modeling and quality control in multidimensional case,' accepted in *Computer Methods in Applied Mechanics and Engineering.*

8 J. Fish, M. Pandheeradi and V.Belsky, 'An efficient multilevel solution scheme for large scale nonlinear systems,' accepted in *Int. J. For Numerical Methods In Engineering.*

9 V. Belsky, 'A Multigrid method for variational inequalities in contact problems,' *Computing*, Vol. 51, pp. 293-311, 1993.

10 C. Farhat and N. Sobh, 'A coarse/fine preconditioner for very ill-conditioned finite element problems,'*Int. J. For Numerical Methods In Engineering*, Vol. 28, pp.1715-1723, 1989.

11 J. Fish and R. Guttal, 'The p-version of the finite element method for shell analysis. Part II: hierarchical quadrature and solution procedures,' submitted to *Computational Mechanics: The International Journal.*

12 N. Carpenter, H. Stolarski and T. Belytschko, 'A Flat Triangular Shell Element With Improved Membrane Interpolation,' *Communications In Applied Numerical Methods,*

VOL. 1, 161-168, 1985.

13 J. Fish and T. Belytschko, 'Stabilized Rapidly Convergent 18-Degrees-of-Freedom Flat Shell Triangular Element,' *Int. J. For Numerical Methods In Engineering*, VOL. 33, 149-162, 1992.

14 J. Batoz, 'A Study of Three-Node Triangular Plate Bending Elements,' *Int. J. For Numerical Methods In Engineering*, VOL. 15, 1771-1812, 1980.

15 D.J. Allman, 'A compatible triangular element including vertex rotations for plane elasticity analysis,' *Computers and Structure*, Vol. 19, pp. 1-8, 1984.

16 K.C. Park and G.M. Stanley, 'A curved C^0 shell element based on assumed natural coordinate strains,' *Journal of Applied Mechanics*, Vol. 108, pp. 278-290, 1986.

17 R. Lohner and K. Morgan, 'An Unstructured Multigrid Method for Elliptic Problems,' *Int. J. For Numerical Methods In Engineering*, VOL. 24, 101-115, 1987.

18 O. Axelson and V.A. Barker, *Finite Element Solution of Boundary Value Problems*, Academic Press, NY, 1984.

19 M.A. Badourah, O.O. Storaasli and S.W. Bostic, 'Linear static structural and vibration analysis on high-performance computers,' *Computer Systems in Engineering*, Vol. 4, pp. 363-371, 1993.

APPENDIX

A. Flat Triangular Shell Element Shape Functions

The DKT plate element shape functions corresponding to the rotational degrees-of-freedom $H_{a'}^{\beta_1}$ and $H_{a'}^{\beta_2}$ are given below [14]:

$$
\begin{aligned}
H_1^{\beta_1} &= 1.5\,(a_6N_6 - a_5N_5) & H_2^{\beta_1} &= b_5N_5 + b_6N_6 \\
H_3^{\beta_1} &= N_1 - c_5N_5 - c_6N_6 & H_1^{\beta_2} &= 1.5\,(d_6N_6 - d_5N_5) \\
H_2^{\beta_2} &= -N_1 + e_5N_5 + e_6N_6 & H_3^{\beta_2} &= -(b_5N_5 + b_6N_6)
\end{aligned}
\tag{39}
$$

where N_i are standard 6-node triangular element shape functions, and

$$
\begin{aligned}
a_k &= -x_{ij}/l_{ij}^2 \qquad b_k = \frac{3}{4}x_{ij}y_{ij}/l_{ij}^2 \qquad c_k = \left(\frac{1}{4}x_{ij}^2 - \frac{1}{2}y_{ij}^2\right)/l_{ij}^2 \\
d_k &= -y_{ij}/l_{ij}^2 \qquad e_k = \left(\frac{1}{4}y_{ij}^2 - \frac{1}{2}x_{ij}^2\right)/l_{ij}^2 \\
l_{ij}^2 &= x_{ij}^2 + y_{ij}^2 \qquad x_{ij} = x_i - x_j \qquad y_{ij} = y_i - y_j
\end{aligned}
\tag{40}
$$

where $k = 4, 5, 6$ for the sides $ij = 23, 31, 12$ respectively. The functions $H_4^{\beta_1}$, $H_5^{\beta_1}$, $H_6^{\beta_1}$, $H_4^{\beta_2}$, $H_5^{\beta_2}$, and $H_6^{\beta_2}$ are obtained from the above expressions by replacing N_1 by N_2 and indices 6

and 5 by 4 and 6, respectively. The functions $H_7^{\beta_1}$, $H_8^{\beta_1}$, $H_9^{\beta_1}$, $H_7^{\beta_2}$, $H_8^{\beta_2}$, and $H_9^{\beta_2}$ are obtained by replacing N_1 by N_3 and indices 6 and 5 by 5 and 4, respectively

Following construction given in equation (10) the out-of-plane displacement shape functions $H_{a'}^{w}$ are given by

$$
\begin{aligned}
H_1^w &= 1-\xi-\eta & H_2^w &= \frac{1}{2}(1-\xi-\eta)\,(-y_{12}\xi + y_{31}\eta) \\
H_3^w &= \frac{1}{2}(1-\xi-\eta)\,(x_{12}\xi - x_{31}\eta) & H_4^w &= \xi \\
H_5^w &= \frac{1}{2}\xi\,[-y_{23}\eta + y_{12}(1-\xi-\eta)\,] & H_6^w &= \frac{1}{2}\xi\,[x_{23}\eta - x_{12}(1-\xi-\eta)\,] \\
H_7^w &= \eta & H_8^w &= \frac{1}{2}\eta\,[-y_{31}(1-\xi-\eta) + y_{23}\xi] \\
H_9^w &= \frac{1}{2}\eta\,[x_{31}(1-\xi-\eta) - x_{23}\xi]
\end{aligned}
\tag{41}
$$

where ξ and η are the area coordinates.

The DMT element shape functions $H_{a'}^{u}$ and $H_{a'}^{v}$ are given as in [15]

$$
\begin{aligned}
H_1^u &= 1-\xi-\eta & H_2^u &= 0 & H_3^u &= \frac{1}{2}(1-\xi-\eta)\,(\xi y_{12} - \eta y_{31}) \\
H_4^u &= \xi & H_5^u &= 0 & H_6^u &= \frac{1}{2}\xi\,[-(1-\xi-\eta)\,y_{12} + \eta y_{23}] \\
H_7^u &= \eta & H_8^u &= 0 & H_9^u &= \frac{1}{2}\eta\,[-\xi y_{23} + (1-\xi-\eta)\,y_{31}]
\end{aligned}
\tag{42}
$$

and

$$
\begin{aligned}
H_1^v &= 0 & H_2^v &= 1-\xi-\eta & H_3^v &= \frac{1}{2}(1-\xi-\eta)\,(-\xi x_{12} + \eta x_{31}) \\
H_4^v &= 0 & H_5^v &= \xi & H_6^v &= \frac{1}{2}\xi\,[(1-\xi-\eta)\,x_{12} - \eta x_{23}] \\
H_7^v &= 0 & H_8^v &= \eta & H_9^v &= \frac{1}{2}\eta\,[\xi x_{23} - (1-\xi-\eta)\,x_{31}]
\end{aligned}
\tag{43}
$$

The shape functions for the drilling degrees-of-freedom $H_{a'}^{\theta}$ are given by

$$
\begin{aligned}
H_1^{\theta} &= \frac{3}{2}\left(-N_4 y_{12}/l_{12}^2 + N_6 y_{31}/l_{31}^2\right) & H_2^{\theta} &= \frac{3}{2}\left(N_4 x_{12}/l_{12}^2 - N_6 x_{31}/l_{31}^2\right) \\
H_3^{\theta} &= N_1 - \frac{1}{4}(N_4 + N_6) & H_4^{\theta} &= \frac{3}{2}\left(N_4 y_{12}/l_{12}^2 - N_5 y_{23}/l_{23}^2\right) \\
H_5^{\theta} &= \frac{3}{2}\left(-N_4 x_{12}/l_{12}^2 + N_5 x_{23}/l_{23}^2\right) & H_6^{\theta} &= N_2 - \frac{1}{4}(N_4 + N_5) \\
H_7^{\theta} &= \frac{3}{2}\left(N_5 y_{23}/l_{23}^2 - N_6 y_{31}/l_{31}^2\right) & H_8^{\theta} &= \frac{3}{2}\left(-N_5 x_{23}/l_{23}^2 + N_6 x_{31}/l_{31}^2\right) \\
H_9^{\theta} &= N_3 - \frac{1}{4}(N_6 + N_5)
\end{aligned}
\tag{44}
$$

B. Shape Function for ANS Shell Element

Interpolants for the rotational field directly follow from equations (19), (20), (21).

$$
\begin{aligned}
N_a^{\theta_{11}}(x_A) &= \frac{h_a}{h_A} N_a \left(e_{a2}^f(1)\, e_{A2,x} + e_{a2}^f(2)\, e_{A2,y} + e_{a2}^f(3)\, e_{A2,z} \right) \\
N_a^{\theta_{12}}(x_A) &= -\frac{h_a}{h_A} N_a \left(e_{a1}^f(1)\, e_{A2,x} + e_{a1}^f(2)\, e_{A2,y} + e_{a1}^f(3)\, e_{A2,z} \right) \\
N_a^{\theta_{21}}(x_A) &= -\frac{h_a}{h_A} N_a \left(e_{a2}^f(1)\, e_{A1,x} + e_{a2}^f(2)\, e_{A1,y} + e_{a2}^f(3)\, e_{A1,z} \right) \\
N_a^{\theta_{22}}(x_A) &= \frac{h_a}{h_A} N_a \left(e_{a1}^f(1)\, e_{A1,x} + e_{a1}^f(2)\, e_{A1,y} + e_{a1}^f(3)\, e_{A1,z} \right)
\end{aligned}
\tag{45}
$$

TABLE 1. Cylinder Mesh Information

Mesh Type	Num. Nodes R dir	Num. Nodes Y dir
mesh 1	21	21
mesh 2	31	31
mesh 3	41	41
mesh 4	61	61

TABLE 2. Three Cylinder Assembly Mesh Information

Mesh Type	Num. Nodes R dir	Num. Nodes Y dir
mesh 1	25	25
mesh 2	31	31
mesh 3	49	49
mesh 4	61	61

TABLE 3. Comparison of Intergrid Transfer Operators for Flat Shell Triangular element (Pinched cylinder with end diaphragms problem. Incomplete Cholesky Smoothing, 2-parameter Acceleration)

Mesh coarse/fine	Intergrid Transfer	thick/span 1/50	thick/span 1/100	thick/span 1/200	thick/span 1/500	thick/span 1/1000
mesh 1/ 3	Bln-Mln	119.8/ 19	124.7/ 21	139.3/ 28	203.4/ 53	302.5/ 99
	Bsh-Msh	97.1/ 10	99.3/ 11	119.8/ 19	137.1/ 26	181.4/ 43
	Bsh-Mln	93.6/ 8	101.8/ 9	119.0/ 17	139.5/ 26	183.4/ 44
	Bln-Msh	124.8/ 20	128.0/ 21	144.6/ 27	210.2/ 53	326.7/ 99
mesh 2/ 4	Bln-Mln	321.4/ 20	317.4/ 20	331.6/ 22	386.3/ 31	521.7/ 57
	Bsh-Msh	278.2/ 11	281.2/ 11	282.4/ 12	326.6/ 18	391.0/ 30
	Bsh-Mln	257.3/ 8	251.2/ 7	265.7/ 10	320.8/ 18	384.0/ 30
	Bln-Msh	324.6/ 20	325.8/ 20	349.9/ 22	394.9/ 31	564.2/ 57

TABLE 4. Comparison of Intergrid Transfer Operators for Flat Shell Triangular element (Pinched Three Cylinder Assembly with end diaphragms problem. Incomplete Cholesky Smoothing, 2-parameter Acceleration)

Mesh coarse/fine	Intergrid Transfer	thick/span 1/50	thick/span 1/100	thick/span 1/200	thick/span 1/500	thick/span 1/1000
mesh 1/ 3	Bln-Mln	213.8/ 19	205.5/ 20	214.6/ 22	287.5/ 43	559.0/ 123
	Bsh-Msh	181.0/ 10	188.7/ 11	184.9/ 13	231.3/ 23	402.8/ 65
	Bsh-Mln	165.4/ 7	168.8/ 9	170.2/ 10	217.1/ 23	394.9/ 68
	Bln-Msh	229.1/ 19	226.2/ 20	221.3/ 24	309.0/ 43	648.2/ 124
mesh 2/ 4	Bln-Mln	361.1/ 20	369.4/ 20	371.7/ 22	457.2/ 37	752.0/ 88
	Bsh-Msh	320.5/ 11	318.0/ 11	338.9/ 12	395.2/ 21	566.9/ 47
	Bsh-Mln	298.0/ 7	304.5/ 8	344.2/ 10	383.1/ 21	564.5/ 47
	Bln-Msh	393.0/ 19	385.5/ 20	393.0/ 21	480.7/ 34	860.5/ 90

TABLE 5. Comparison of Intergrid Transfer Operators for ANS Shell element (Pinched cylinder with end diaphragms problem. Incomplete Cholesky Smoothing, 2-parameter Acceleration)

Mesh coarse/fine	Intergrid Transfer	thick/span 1/50	thick/span 1/100	thick/span 1/200	thick/span 1/500	thick/span 1/1000
mesh 1/ 3	BiQ9	297.9/ 14	341.1/ 26	423.0/ 51	656.5/ 128	1028.6/ 245
	BiQ9Mr	306.8/ 14	353.9/ 26	450.0/ 51	748.0/ 129	1207.0/ 247
	BiL4	366.0/ 19	430.0/ 36	569.6/ 72	975.6/ 176	1581.0/ 328
	MeBiL4	438.8/ 9	467.1/ 13	645.6/ 21	711.9/ 40	747.4/ 66
	BiQ9Re	270.6/ 10	301.2/ 16	357.3/ 30	536.3/ 79	975.9/ 188
mesh 2/ 4	BiQ9	728.8/ 10	775.0/ 18	905.7/ 34	1283.0/ 83	1895.6/ 167
	BiQ9Mr	753.6/ 11	845.1/ 18	965.7/ 34	1413.6/ 84	2153.8/ 168
	BiL4	929.1/ 13	1056.0/ 24	1260.8/ 48	1993.3/ 121	3160.6/ 242
	MeBiL4	1401.1/ 8	1450.6/ 10	1453.4/ 15	1651.5/ 28	1874.7/ 45
	BiQ9Re	664.9/ 8	672.7/ 12	773.0/ 20	1024.0/ 50	1581.4/ 111

TABLE 6. Comparison of Intergrid Transfer Operators for ANS Shell element (Pinched Three Cylinder Assembly with end diaphragms problem. Incomplete Cholesky Smoothing, 2-parameter Acceleration)

Mesh coarse/fine	Intergrid Transfer	thick/span 1/50	thick/span 1/100	thick/span 1/200	thick/span 1/500	thick/span 1/1000
mesh 1/ 3	BiQ9	449.8/ 12	490.6/ 22	601.5/ 42	867.9/ 103	1340.9/ 200
	BiQ9Mr	467.3/ 12	514.3/ 22	618.1/ 43	981.2/ 103	1564.8/ 203
	BiL4	772.3/ 48	931.1/ 80	1319.0/ 139	2230.8/ 298	> 300
	MeBiL4	966.0/ 38	1126..7/ 59	1350.7/ 86	1856.9/ 153	> 400
	BiQ9Re	413.0/ 11	456.5/ 18	521.7/ 30	835.6/ 77	1365.1/ 164
mesh 2/ 4	BiQ9	729.6/ 11	762.6/ 18	972.8/ 35	1398.1/ 86	1937.1/ 164
	BiQ9Mr	777.3/ 11	819.8/ 19	982.3/ 36	1421.5/ 87	2194.7/ 165
	BiL4	1239.9/ 47	1482.77/ 70	2141.3/ 140	3739.6/ 292	> 300
	MeBiL4	1802.0/ 39	2033.9/ 54	2468.5/ 92	3543.3/ 156	3765.8/ 186
	BiQ9Re	681.2/ 10	733.4/ 14	834.6/ 25	1163.1/ 64	1767.3/ 131

TABLE 7. Comparason of acceleration schemes for Flat Shell Triangular element (Pinched cylinder with end diaphragms problem. Incomplete Cholesky Smoothing)

Mesh coarse/fine	Accel. Type	thick/span 1/50	thick/span 1/100	thick/span 1/200	thick/span 1/500	thick/span 1/1000
mesh 1/ 3	case 1	119.4/ 11	147.8/ 18	232.7/ 37	588.0/ 127	1481.7/ 354
	case 2	93.6/ 8	101.8/ 9	119.0/ 17	139.5/ 26	183.4/ 44
	case 3	92.5/ 8	94.4/ 9	113.8/ 17	138.3/ 26	185.3/ 44
mesh 2/ 4	case 1	336.6/ 14	313.4/ 12	392.2/ 20	779.9/ 61	1760.5/ 166
	case 2	257.3/ 8	251.2/ 7	265.7/ 10	320.8/ 18	384.0/ 30
	case 3	250.1/ 8	247.0/ 7	265.0/ 10	311.2/ 18	384.0/ 30

Note: case 1: without acceleration; case 2: two-parameter acceleration; case 3: CG acceleration.

TABLE 8. Comparason of acceleration schemes for ANS element (Pinched cylinder with end diaphragms problem. Incomplete Cholesky Smoothing)

Mesh coarse/fine	Accel. Type	thick/span 1/50	thick/span 1/100	thick/span 1/200	thick/span 1/500	thick/span 1/1000
mesh 1/ 3	case 1	538.1/ 45	2074.1/ 159	/>500	/ >1000	/>1000
	case 2	297.9/ 14	341.1/ 26	423.0/ 51	656.5/ 128	1028.6/ 245
	case 3	300.9/ 14	336.9/ 26	417.7/ 51	674.5/ 128	1054.5/ 245
mesh 2/ 4	case 1	1028.5/ 23	1656.9/ 73	4234/ 273	/>1000	/>1000
	case 2	728.8/ 10	775.0/ 18	905.7/ 34	1283.0/ 83	1895.6/ 167
	case 3	716.0/ 10	790.9/ 18	937.6/ 34	1290.8/ 83	1929.5/ 167

Note: case 1: without acceleration; case 2: two-parameter acceleration; case 3: CG acceleration.

TABLE 9. Comparison of smoothing procedures for Flat Shell Triangular element (Pinched cylinder with end diaphragms problem. Two-parameter acceleration)

Mesh coarse/fine	Smoothing Procedure	thick/span 1/50	thick/span 1/100	thick/span 1/200	thick/span 1/500	thick/span 1/1000
mesh 1/ 3	MIC	93.6/ 8	101.8/ 9	119.0/ 17	139.5/ 26	183.4/ 44
	1 GS	109.9/ 14	114.5/ 16	157.3/ 32	340.8/ 101	697.1/ 235
	2 GS	106.4/ 9	113.6/ 11	144.1/ 18	260.8/ 46	544.6/ 114
mesh 2/ 4	MIC	257.3/ 8	251.2/ 7	265.7/ 10	320.8/ 18	384.0/ 30
	1 GS	293.3/ 14	302.4/ 15	344.9/ 21	570.5/ 57	1215.0/ 160
	2 GS	295.5/ 9	294.6/ 9	328.5/ 13	459.6/ 28	829.3/ 63

TABLE 10. Comparison of smoothing procedures for ANS element (Pinched cylinder with end diaphragms problem. Two-parameter acceleration)

Mesh coarse/fine	Smoothing Procedure	thick/span 1/50	thick/span 1/100	thick/span 1/200	thick/span 1/500	thick/span 1/1000
mesh 1/ 3	MIC	297.9/ 14	341.1/ 26	423.0/ 51	656.5/ 128	1028.6/ 245
	1 GS	371.8/ 32	538.7/ 82	1092.8/ 244	/ >300	/ >300
	2 GS	369.1/ 22	521.4/ 47	1060.7/ 140	/ >300	/ >300
mesh 2/ 4	MIC	728.8/ 10	775.0/ 18	905.7/ 34	1283.0/ 83	1895.6/ 167
	1 GS	812.7/ 22	995.4/ 43	1749.7/ 136	/ >300	/ >300
	2 GS	809.4/ 14	1032.5/ 29	1732.4/ 80	/ >300	/ >300

TABLE 11. Comparison of solution methods for flat shell triangular element (Pinched cylinder with end diaphragms problem)

Mesh coarse/fine	Slover Type	thick/span 1/50	thick/span 1/100	thick/span 1/200	thick/span 1/500	thick/span 1/1000
mesh 2/ 4	two-grid	257.3/ 8	251.2/ 7	265.7/ 10	320.8/ 18	384.0/ 30
	PCG	1088.7/ 427	977.8/ 372	1231.1/ 485	> 500	> 500
	direct	864.8				

TABLE 12. Comparison of solution methods for ANS element (Pinched cylinder with end diaphragms problem)

Mesh coarse/fine	Slover Type	thick/span 1/50	thick/span 1/100	thick/span 1/200	thick/span 1/500	thick/span 1/1000
mesh 2/ 4	two-grid	664.9/ 8	672.7/ 12	773.0/ 20	1024.0/ 50	1581.4/ 111
	PCG	1580.7/ 314	2170.8/ 474	> 500	> 500	> 500
	direct	1490.3				

TABLE 13. Comparison of solvers for graded meshes (Pinched cylinder with end diaphragms problem with thick/span 1/100. Two-parameter acceleration)

Solver Type	FST	ANS
two grid (2grd/ 3grd)	326.9/ 8	1701.7/ 53
direct	484.4	2278.7
three grid (1grd/2grd/ 3grd)	326.8/ 20	2846.4/ 163
direct	484.4	2278.7

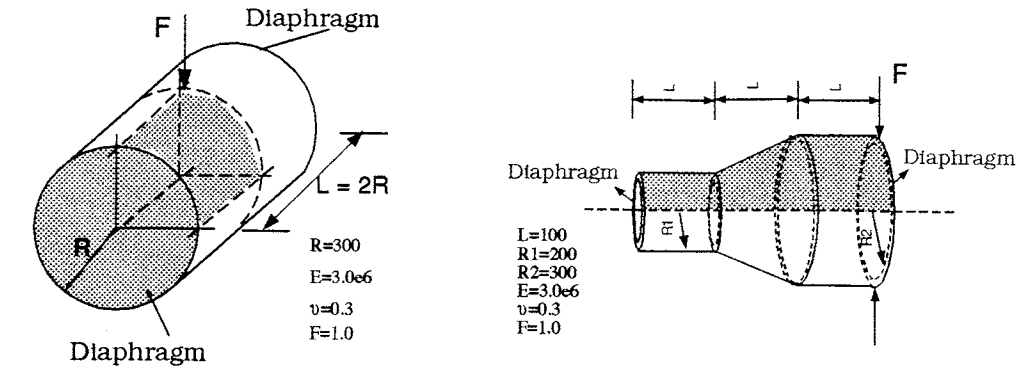

(a). Pinched cylinder with end diaphragms

(b). Assembly of three cylinders with end diaphragms

FIGURE 1. Geometry, boundary conditions, material properties

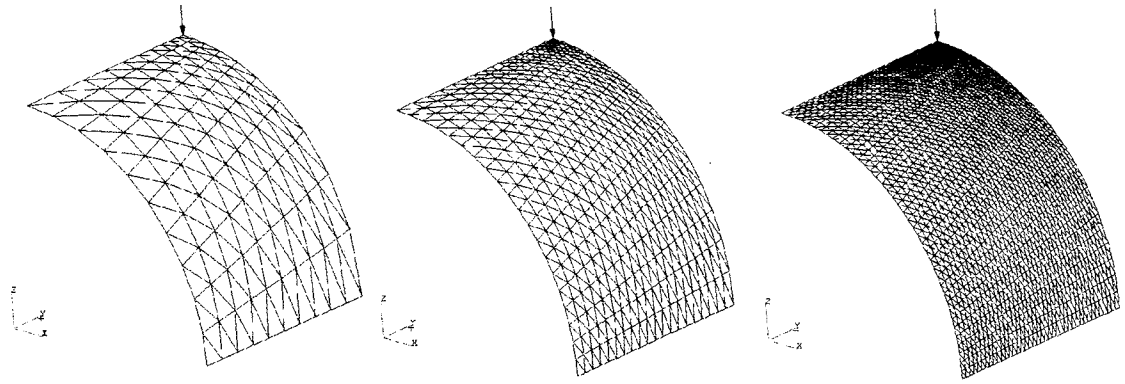

Mesh 1grd **Mesh 2grd** **Mesh 3grd**

FIGURE 2. Graded mesh information (Flat shell trangular)

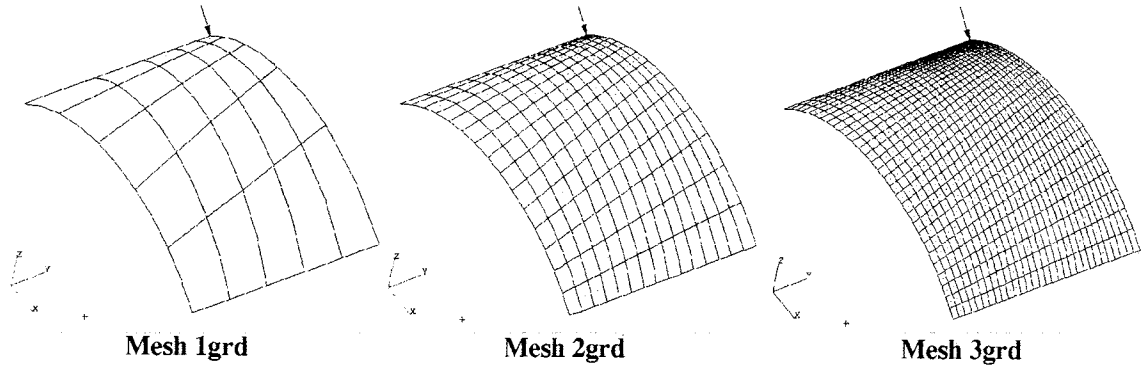

Mesh 1grd **Mesh 2grd** **Mesh 3grd**

FIGURE 3. Graded mesh information (Quadrilateral shell element)